Photovoltaic modules designed for architectural integration without negative performance consequences

M.C. López-Escalante[1*], E. Navarrete-Astorga[2], M.Gabás[2], J.R. Ramos- Barrado[2] and F. Martín[1]

[1]The Nanotech Unit, Laboratorio de Materiales y Superficies and Departamento de Ingeniería Química, Facultad de Ciencias, Universidad de Málaga, Málaga, 29071, Spain.

[2]The Nanotech Unit, Laboratorio de Materiales y Superficies and Departamento de Física
Aplicada I, Facultad de Ciencias, Universidad de Málaga, Málaga, 29071, Spain.

Abstract

Nowadays, the photovoltaic technology level development makes it the best option for its building integration as energy supplier. Nevertheless, its aesthetic appearance plays a relevant role because architect requirements go beyond the simple installation of solar devices on terraces. In order to fulfill their requirements, the typical white backsheet uses to be replaced by a black one. This simple change leads to a huge PV module performance reduction. In this work, it has been demonstrated that a suitable material selection allows to fabricate photovoltaic modules with a high architectonic integration, but without power reduction with respect to the most commercial solar devices. The former consists in the replacement of the typical glass front cover and the white backsheet by an antireflective glass and a black backsheet respectively. All the study has been developed on real size photovoltaic modules fabricated in an automatic line. The obtained results determine that those modules where black backsheets are used, suffer a power reduction equal to 8.66 W per fabricated module. Nevertheless, when in addition of the black backsheet an antireflective coating glass is implemented, the resulted PV modules present a more aesthetic presence without a detrimental of their power performance when they are compared to the standard PV modules. Additionally, the fabricated solar devices using the proposed configuration successfully overcome the most common aging tests.

Keywords: architectural integration, power balance, novel material design, silicon photovoltaic module, antireflective coating, black backsheet

1 Introduction

The global economy is growing at an average rate of 3.4% per year and the population will expand from 7.4 to 9 billion people by 2040 [1,2]. Obviously, the upward trend of these two parameters will be associated with a hard urbanization process and an increase in the energy consumption. According to several authors, this process will imply 30% and 60% rises, respectively, in energy and electricity demand in buildings [1,2,3]. Taking into account these perspectives and in order to meet the Paris Agreement, the energy sector will face a great challenge in which renewable energies should continue improving their technological efficiency and profitability.

Several approaches are actually active in order to promote the development of renewable energies as energy supply to urban environments. The purpose is to bring them closer to cities aiming to be self-sustainables from an energy point of view [4,5]. In the particular case of photovoltaic (PV) energy, the absence of noise and mobile parts together with the high possibility of easy management as construction elements, has promoted its integration in buildings and other simple structures like pergolas. [6,7]. Actually, the main approach is the building integrated photovoltaic (named as BIPV), That is, photovoltaic components are steering from "building-applied" to "building-integrated" systems [8,9]. Despite its energy benefits, BIPV is not exempt from other environmental problems such as urban heat islands (UHI). UHI phenomenon is related with anthropogenic heating of urban area when compared to its surrounding rural areas Bao-Jie He. *Towards the next generation of green building for urban heat island mitigation: Zero UHI impact building. Sustainable Cities and Society 50 (2019) 101647; M. Zinzi, S. Agnoli. Cool and green roofs. An energy and comfort comparison between passive cooling and mitigation urban heat island techniques for residential buildings in the Mediterranean region. Energy and Buildings 55 (2012) 66-76]*. BIPV are included among these activities because PV modules are designed to absorb the solar radiation, therefore their large-scale deployment inside cities leads to a negative climate impact *[Miguel Centeno Brito. Assessing the impact of photovoltaics on rooftops and facades in the urban micro-climate. Energies 13 (2020) 2717; Anthony Dominguez, Jan Kleissl, Jeffrey C. Luvall. Effects of solar photovoltaics panels on roff heat transfer. Solar Energy 85 (2011) 2244-2255; Nitin Shukla, Alliston Watts, Christian Honeker, Mark Hill, Jan Kosny. Thermal impact of adhesive-mounted rooftop PV on underlying roof shingles. Solar Energy 174 (2018) 957-966; Julie V. Pham, Amir Baniassadi ,Kyle E. Brown, Jannik Heusinger, David J. Sailor. Comparing photovoltaic and reflective shaded surfaces in the urban environment: Effects on surface sensible heat flux and pedestrian thermal comfort. Urban Climate 29 (2019) 100500]*. The associated temperature increment to UHI effect drives to higher energy and water demand, and it is related with a significant impact on human health, in particular during heat waves.

With the objective of adapting to the different needs of the market and trying to minimize the negative effects that they can produce, offered BIPV products use to be grouped in five categories *[Akash Kamur Shukla, K. Sudhakar, Prashant Baredar. Recent advancement in BIPV product technologies: A review. Energy and Buildings 140 (2017) 188-195; Alessandra Scognamiglio, Harald N Rostvik. Photovoltaics and zero energy buildings: a new opportunity and challenge for design. Progress in photovoltaics: research and applications 21, 2013, 1319-1336; Meng Li, Tao M, Jianying Liu, Huanhuan Li, Yaling Xu, Wenbo Gu, Lu Shen. Numeral and experimental investigation of precast concrete façade integrated with solar photovoltaic panels. Applied Energy 253, 2019, 13509]*: (1) foil devices characterized by their light weight and flexibility are a suitable option for curved architectural shells *[Bjorn Petter Jelle, Chister Breivik, Hilde Drolsum Rokenes. Building integrated photovoltaic products: A state-of-the-art review and future research opportunities. Solar Energy Materials and Solar Cells 2012, 100, 69-96]*; (2) tile shape products which join a high performance with a low weight making them the best solution for residential pitched roofs; (3) module devices, the most competitive product with high efficiently performance and easy to handle *[Marc J. R. Perez, Vasilis Fthenakis, Hyung-Chul Kim, Anthony O. Pereira. Façade-integrated photovoltaics: a life cycle and performance assessment case study. Progress in Photovoltaic: research and applications 20, 2012, 975-990]*; (4) semitransparent systems which most applied in prestigious buildings with well-visible facades and skylights due to their high aesthetic level *[Jinqing Peng, Dragan C. Curcija, Anothai Thanachareonkit,*

Eleanor S. Lee, Howdy Goudey, Stephe E. Selkowitz. Study on the overall energy performance of a novel c-Si based semitransparent solar photovoltaic window. Applied Energy 242, 2019, 854-872; Hyo Mun Lee, Jong Ho Yoon. Power performance analysis of a transparent DSSC BIPV window based on 2 year measurement data in a full-scale mock-up. Applied Energy 225, 2018, 1013-1021] and finally, (5) building applied/attached PV (BAPV) products which use to be incorporated as external building walls and curtain walls due to their different colors and visual effects *[Anishkumar Soman Anthony. Colored solar cells with spectrally selective photonic crystal reflectors for application in building integrated photovoltaics. Solar Energy 181 (2019) 1-8; Chin-Ti Tsai, Chin-Yao Tsai. See-thourgh, light-though, and color modules for large-area tandem amorphous/microcrystalline silicon thin-film solar modules: Technology development and practical considerations for building-integrated photovoltaic applications. Renewable Energy, 145 (2020) 2637-2646]*

All these devices can be classified as PV modules,.Within th~~is~~ concept~~,~~ though the incorporation of novel solar cell concepts such as organic-based ones [10], or concentration systems [11] are gaining ground, workhorse is still based on c-Si flat modules.

Concerning c-Si flat modules, the main efforts made so far have been focused on the PV module engineering and efficiency aspects, moving to a second level almost everything related to its aesthetic aspect. Most of the produced modules have their dark blue solar cells on a white background which does not usually meet the aesthetic requirements imposed by architects and designers, endangering the diffusion and consolidation of BIPV technology [12,13,14,15].

Regarding to an aesthetic PV module, up to now the most common adopted solution is the replacement of the rear white backsheet by a black one which use to be accompanied by a black frame too [9]. These changes lead to a sophisticated PV module with a really good acceptance by architects [16]. Nevertheless, the electrical performance of these aesthetic PV modules is highly penalized because the radiation reflected by white backsheet areas is annulled. Factory engineers are aware of this behavior, which is why the highest power photovoltaic cells are selected to manufacture these black photovoltaic modules, with the aim to obtain solar devices with a competitive output power value. Obviously, if the aesthetic PV module price is not conveniently increased, their production would be able to lead to a factory negative economic result [17].

A way to mitigate these power losses is to extend the utility of non-silicon PV module components, i.e. from simple structural elements to active items for solar power generation. In this work, the proposal is to replace the standard outer protective film, this is the textured glass, by another with an antireflective coating (from now on named as AR), with the aim to reduce reflection from the PV module surface and balance the power losses caused by the more aesthetic black backsheet. Until now and in the field of PV, AR coating glass research is focused on the solar device performance improvement, but mainly concerning small modules [18,19,20,21,22]. However, none of these works focus the analysis as a possible solution to the power drop of the aesthetic modules for architectural integration, nor do they perform the aging tests. The latter point (failing the ageing tests) has long been holding back the industrial implementation of AR-coated glass.

According to these premises, in this work we have concentrated our efforts in the analysis of different combinations of front and back PV module materials. The evaluated aspects are the PV module energy performance, its reliability and the associated economic issues. The purpose of this work is to demonstrate that it is possible to balance the power performance reduction due to the black backsheet by means of the use of an AR front

coating glass, which leads to an irradiance reflection reduction. With the aim to give the more useful information as possible, the main part of this work has been developed in real size PV modules, fabricated in an automatic industrial line. Moreover, the most common accelerated aging tests have been carried out to determine their behavior under extreme environmental conditions.

2 Materials and methods

The experimental work has been performed on two different sets of samples depending on the analysis objective. The first set is focused on single samples of the two studied protective covers, backsheet and glass, and the objective is to know their potential improvements in device performance and their stability. Regarding the sample analysis, glass transmittance, backsheet and ethylene vinyl-acetate (EVA) adhesion, EVA gel content and black backsheet ultraviolet stability have been studied. The second part of the experimental work has been carried out over real size PV modules fabricated with the previously analyzed materials, and the objective is to determine their influence over the final output power and the final device reliability.

The first single sample analysis has involved transmittance measurements of standard (STD) glass cover and AR glass cover with two different widths: 3 mm and 4 mm, from now on denoted as STDGlass, 3ARGlass and 4ARGlass respectively [23,24]. In this case, STDGlass has been used as reference. The transmittance measurements of the three glass types have been carried out over real size samples with an USB200 spectrometer for Ocean Optics, specially adapted. Glass technical datasheets indicate that STDGlass, 3ARGlass and 4ARGlass have optical transmittance equals to 91.6%, 94.5% and 94.4% respectively [23]. These values will be compared with those measured by our transmittance tool.

The second single sample analysis evaluates the EVA-backsheet adhesion properties, together with the backsheet mechanical stability by the measurement of the 180º peel test according to ISO 527 normative. For this item, three backsheet-EVA-backsheet sets have been laminated together in a Prosain industrial laminator and after that, they have been cut on ribbon format. This test will give us the tensile strength necessary to separate EVA-backsheet stack, which will be compared with the values shown in the supplier technical datasheet. Moreover, as the own backsheet is composed by several films [25], this test will show us the mechanical stability of this outer protective material. XLW (M) auto tensile tester from Labthink was used for this test. The 180° peel test measurement has been carried out at 100.0 mm/min pull speed. The black backsheet provider indicates that the tensile strength value must be higher than 30 N/cm^2 in any case.

The third single sample analysis evaluates the suitability of the lamination conditions. The gel content test is the most commonly used [26,27]. This analysis determined the EVA cure grade which is directly related with the amount of polymer which has been successfully crosslinked. Industrial typical values indicate that the lamination process conditions are correctly defined when the gel content value is between 65%-90%. In this case, gel content test has been developed with the aim to know if it would be necessary to change the lamination process conditions when the AR@Black combination material overcomes the whole PV module evaluation. Therefore, gel content test will not be used as decisive test for discard some of the two evaluated materials in this work.

The final single sample analysis studies the backsheet stability under ultraviolet radiation. For this item, two samples of backsheet with a size of 5 cm x 10 cm have been

introduced in the ultraviolet laboratory camera from Neurtek company and the aging test has been carried out according to IEC6125 normative [28]. The overcome of this test just obey to visual inspection, therefore images before and after the test have been examined.

The second part of this study has been developed on real size monocrystalline silicon solar cell PV modules, each one containing 60 PV cells. Four different front and back materials combinations have been analyzed in this work. In order to facilitate the material design readable, the following nomenclature will be used: type of glass@type of backsheet. Regarding the former simplification, the glass and backsheet possible combinations are: STD@White, AR@White, STD@Black and AR@Black, as they are gathering in Table 1. Their power and reliability variations due to the new considered materials have been studied. For this item, 10 PV modules per each of the four possible material combinations have been fabricated. Figure 1 shows these four material designs and the performed tests. The selected outer protective film combinations for the forty PV modules production have been: STD@White, STD@Black, AR@White and AR@Black. These forty PV modules have been fabricated in an automatic industrial line. The production line starts with the cleaning of the textured glass (3.2–4.0 mm thickness and 91.6% transmittance) in the case of the STD one. Regarding ARGlass, only 3ARGlass (3.2 mm thickness and 94.5% transmittance) [23] has been incorporated to the industrial line because 4ARGlass optical study revealed a slight decrement in the transmittance value with respect to the reference value (94.4%) [23]. Moreover, the AR Glass manual or mechanical handling implies the use of cotton gloves with the aim to avoid the visual coating deterioration. After that, the EVA front encapsulant foil whose thickness is 460 μm [29] is placed onto the glass. Six solder photovoltaic cell strings (each string is formed by ten solar devices) are disposed over each PV device. The second encapsulant foil (460 mm) [29] and the PET backsheet are added. Twenty of the forty PV modules have been fabricated with white backsheet (295 mm thickness) [25] and the other twenty have been fabricated with the black backsheet following the schema of Figure 1. Then the global stack is processed at the lamination machine. Finally, the connection box is placed and the electrical measurement in an AAA class solar module tester under standard conditions is carried out (according to IEC 60904 [30]) where the main PV module electrical parameters are measured. They are short current intensity (I_{sc}), open circuirt voltage (V_{oc}), intensity, voltage and power at the maximum power point (I_{mp}, V_{mp} and P_{mp}), which allow to calculate the fill factor (FF), and the cell to module ratio (CMR). I-V curve parameter comparison will be very useful to know which electrical parameter is exactly influenced by every changed film. The last production step is the sealing of the photovoltaic module and the anodized aluminium frame (twenty in grey color and twenty with black color) is assembled.

Type of front glass@type of backsheet	**Brief description**
STD@White	industrial PV module standard
AR@White	replacing front glass by glass+AR coating
STD@Black	changing white backsheet for a black one
AR@Black	combination proposed in this work

Table 1. PV modules analyzed in this work.

After that, one module for AR@White and AR@Black combination materials have to overcome the standard accelerated aging test defined by the International Electrotechnical Commission (IEC, specifically IEC 61215 edition 2) [28] or Underwriters Laboratories (UL) [31]. The failure criterion is defined by a power loss higher than 5% after the accelerated aging test. The principal accelerated aging tests are damp heat (DH), thermal cycling (TC) and humidity-freeze (HF), which are carried out with the aim to evaluate the influence of moisture ingress in the laminated structure, the thermo-mechanical stresses in the cell and PV module due to the different thermal expansion coefficients of the various materials within the laminate, and the influence of both mechanisms at the same time. Regarding the relevance of the backsheet on the moisture ingress, the DH test has been carried out in another AR@Black module. Moreover, with the aim to follow the PV module evolution, this aging test has been paused two times before its end, namely at 420 h and 880 h. The accelerated aging test results have been quantitatively evaluated by measuring the I–V curves prior, during (in the case of the progressive DH test), and after each degradation test, and qualitatively evaluated by electroluminescence (EL) images taken with a Sensovation brand camera. Concerning the potential induced degradation test (PID), as the front encapsulant material has not changed, it has not been necessary to carry out it [32].

Finally, in the last results subsection, the production capacity and economic impact of the power enhancement with respect to the traditional material configuration has been analyzed for the four selected designs in a real work environment.

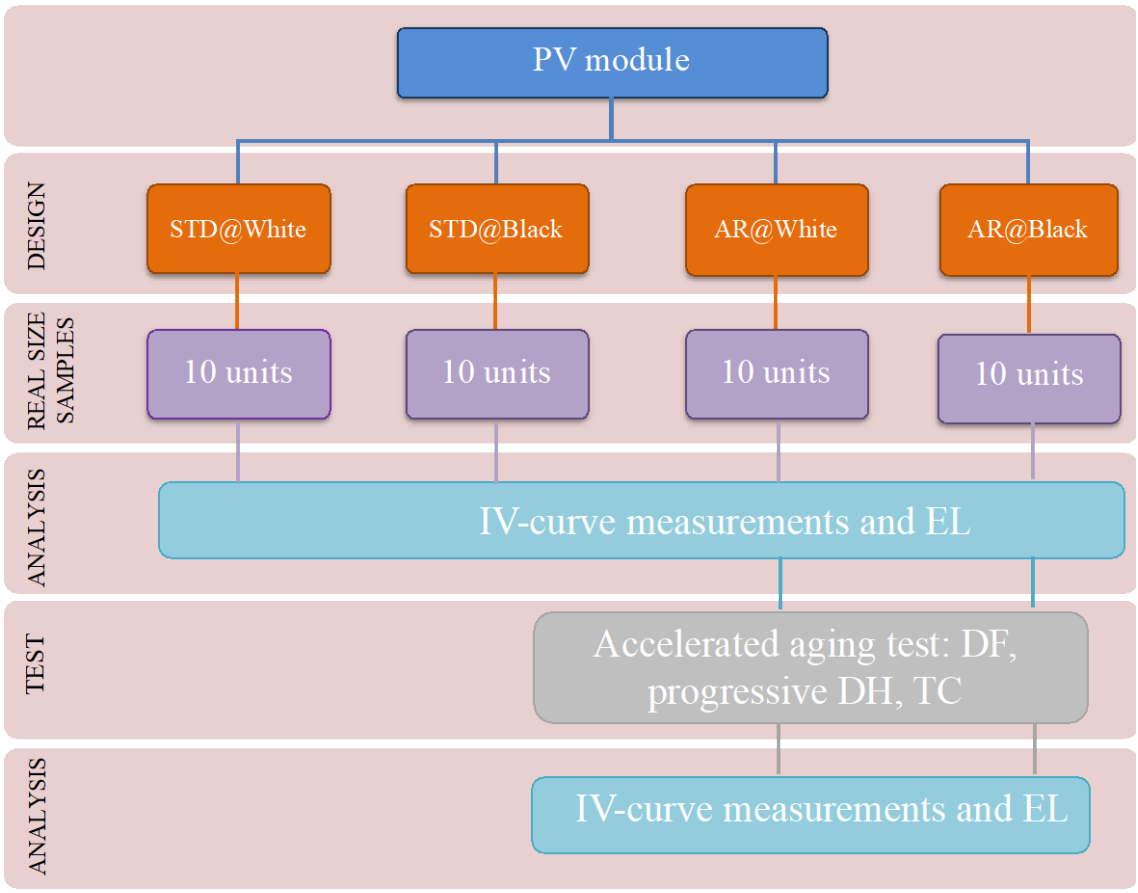

Figure 1. Schema of real size fabricated PV module samples and the experimental measurements done for each material combination

3. Results and discussion

3.1 Analysis of the outer protective films

In this subsection, the measurements taken to characterize the front cover and backsheet materials are presented.

3.1.1 Glass optical study

The PV module glass front cover replacement can imply a substantial modification of the solar radiation (quantity and available spectrum range) that reaches the PV cells. In this study the STDglass is replaced by another one with an AR coating film (ARGlass). The main role of the AR coating is the reduction of the reflected radiation after impinging the PV module front surface. That is, the transmitted radiance quantity to the PV module inner part will be increased when replacing the STDglass by the ARGlass. To quantify this radiation increase, transmittance measurements have been carried out over real size samples of STDGlass of 3.2 mm and ARGlass with two different thicknesses, 3.2 mm (3ARGlass) and 4 mm (4ARGlass). Figure 2 shows the corresponding spectra. The three samples have a similar behavior at the lowest wavelength region, 294 nm to 360 nm, where a strong transmittance value increment can be observed from 4.87% to 92.66%. After that wavelength interval, the transmittance spectra depict horizontal lines for the three analyzed samples. The unique difference between them is related with transmittance value, being the 3ARGlass sample the one

with the higher transmittance value, followed by the 4ARGlass sample and by STDGlass sample. For example, in the visible region, their transmittance values are 95.73%, 93.53% and 87.42% at 700 nm, respectively. These values have to be compared with datasheet transmittance values: 94.5%, 94.4% and 91.6%. These results indicate that fabricated PV modules with the 3ARGlass cover will significantly increase their power generation with respect to those solar devices which will be assembled with STDGlass material. In the case of PV modules with 4ARGlass cover, they will present a moderate power increment mainly due to a higher radiation absorption. These results lead to discard the PV module fabrication with 4ARGlass.

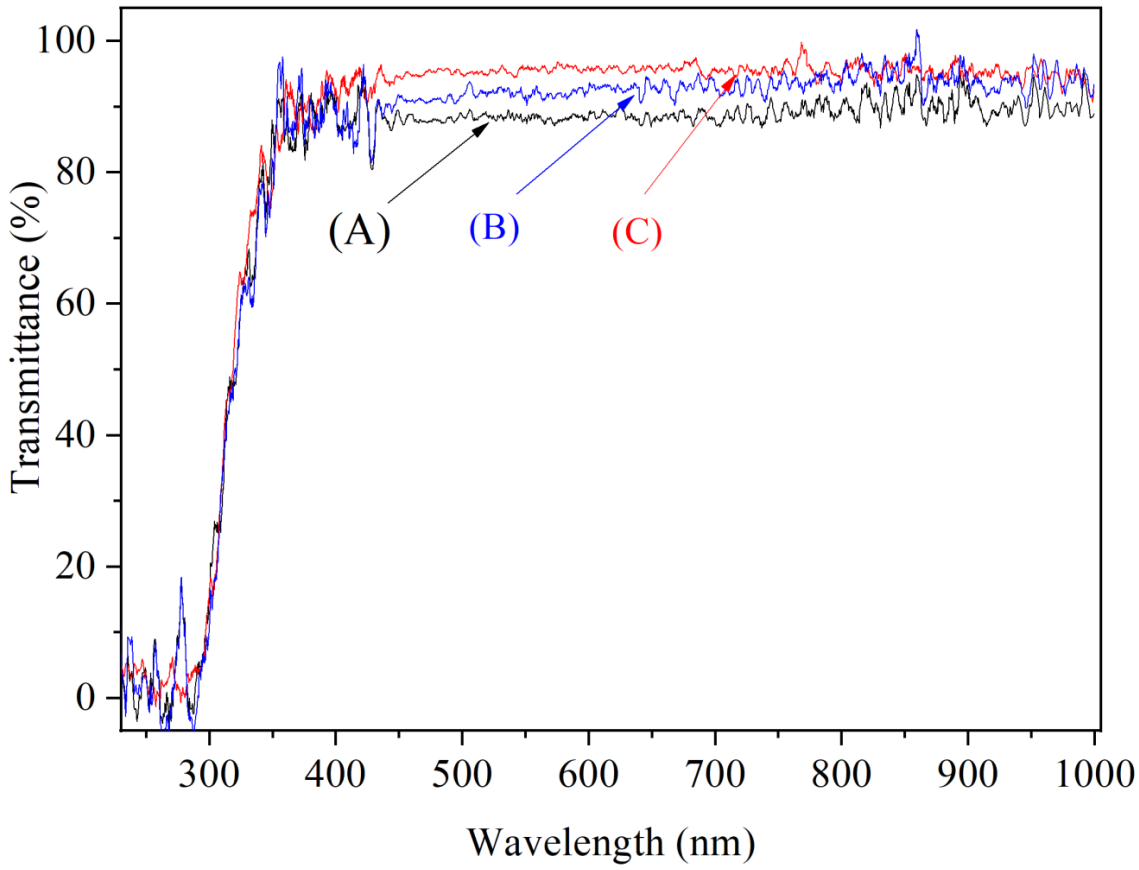

Figure 2. Transmittance spectra for real size glass cover used for production PV module: (A, black line) STDGlass; (B, red line) 3ARGlass; and (C, blue line) 4ARGlass.

3.1.2 Backsheet analysis

The backsheet main function is to chemically isolate the (EVA/PV cell/EVA) stack from the environment. Therefore, it is fundamental to study the adhesion between EVA and the proposed black backsheet because its stability is directly related with the PV module longevity during its whole operational lifetime. In this case, the peel test has been carried out in agreement with the ISO 527 normative. For such purpose, three samples (black backsheet/EVA/black backsheet systems) have been prepared with the same lamination conditions: 145ºC, 300 s, 600 s for temperature, vacuum time and pressure time respectively. Figure 3 shows the applied strength versus the obtained displacement for the three prepared samples. The A profile corresponds to the first

analyzed sample with a total width of 3 cm. The maximum strength is equal to 67.01 N/cm for which an elongation of 10.58 mm has been measured. This implies that the tensile strength value is equal to 63.34 N/cm^2. The other two samples have the same width, 1 cm. Their maximum strengths are 98.36 N/cm and 103.20 N/cm, with a measured displacement of 8.55 mm and 7.20 mm respectively. Therefore, their tensile strength values are equal to 115.04 N/cm^2 and 143.33 N/cm^2 respectively. The supplier technical datasheet indicates that the tensile strength value must be higher than 30 N/cm^2 in any case. This implies that the three samples have overcome this test. The rest of the showed profiles are very similar because after the former point, the strength is relaxed under values around 30 N/cm for A sample and 20 N/cm in the case of B and C samples. Moreover, it is important to indicate that neither of the three samples present any backsheet delamination after the test, as can be seen in the inset images of Figure 3 where the final test images are presented for samples A, B, C. Image C* is a more detailed view of the C sample.

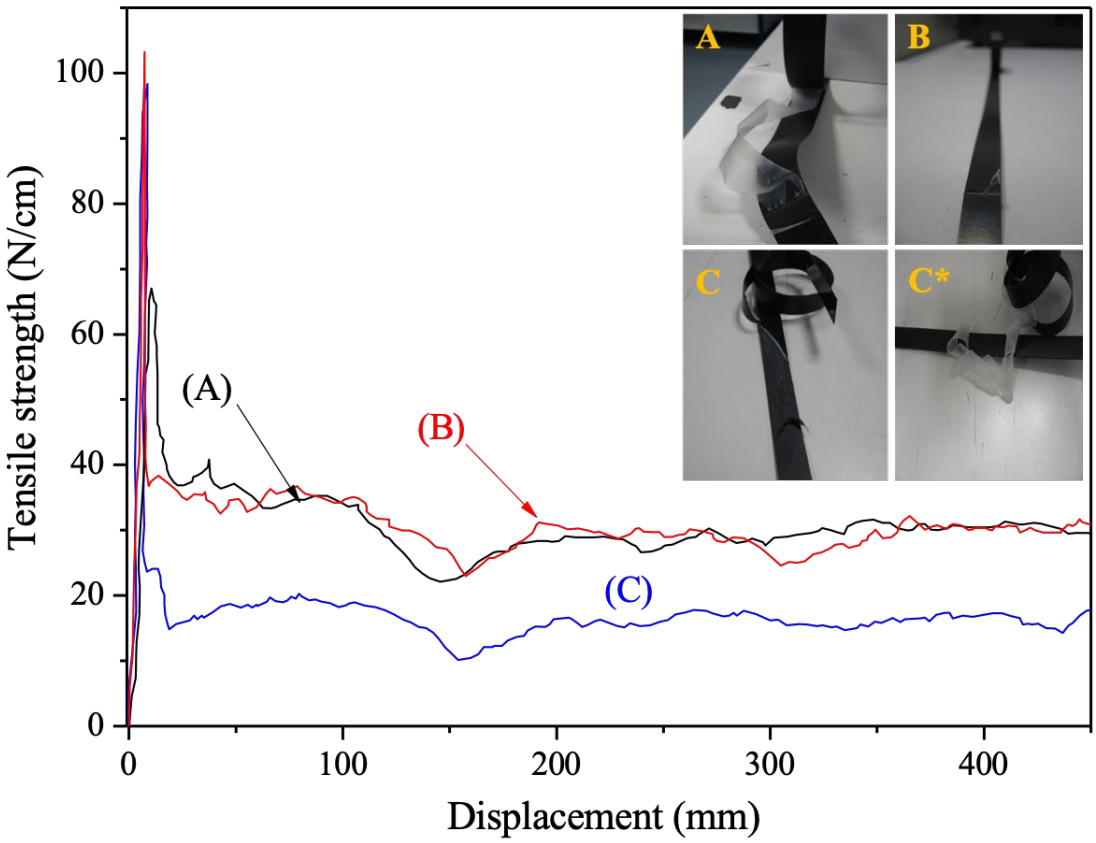

Figure 3. Peel test profile for three different Black Backsheet@EVA@ Black Backsheet: (A) width equal to 3 cm; (B) and (C) width equal to 1 cm. Final result samples are shown in the inset images on the upper right part of the graph.

3.1.3 Gel content and ultraviolet degradation studies

In order to guarantee a suitable PV module lamination which will definitively influence over the solar module longevity, gel content analysis is carried out as a quality control for standard production. This test measures the EVA cure grade, whose typical values range between 65% to 90%. The cure process is a chemical reaction which implies

the crosslink between polymer molecules and it is carried out at the temperature of the lamination process stage. Therefore, the gel content value gives us the EVA material percentage which has successfully reacted. This test is a priority when EVA film suppliers or lamination conditions are changed, with the main objective of determine the EVA quality after lamination. In this case, EVA material is the same, irrespective of the backsheet type, so the test results are no decisive for black backsheet evaluation. Nevertheless, it is suitable to perform it because slight lamination condition variations could be necessary for a high-quality PV module production.

Specific PV modules were fabricated to carry out this gel content test, and then five samples were cut and extracted. Gel content values varied from 39% to 59%, which are lower than the internal quality optimal range (65%-90%). These values indicate that if the material combination will overcome the evaluation and it will be accepted for commercial PV module production, an optimization of the lamination process condition will be required in order to guarantee PV module lifetime.

The UV degradation study has been carried out over two single black backsheet samples according to IEC 61215 normative at an UV laboratory chamber. Figure 4 shows images for these samples before and after the UV degradation. Figure 4A and 4B show the inner face film which will be in contact with the rear EVA foil, before and after the UV degradation respectively. Figure 4C and 4D present the outer face film which will be exposed to the ambient, before and after the degradation respectively. As can be observed, neither of the two samples present a visual degradation because they do not present color degradation, bubbles or any type of aesthetic defect.

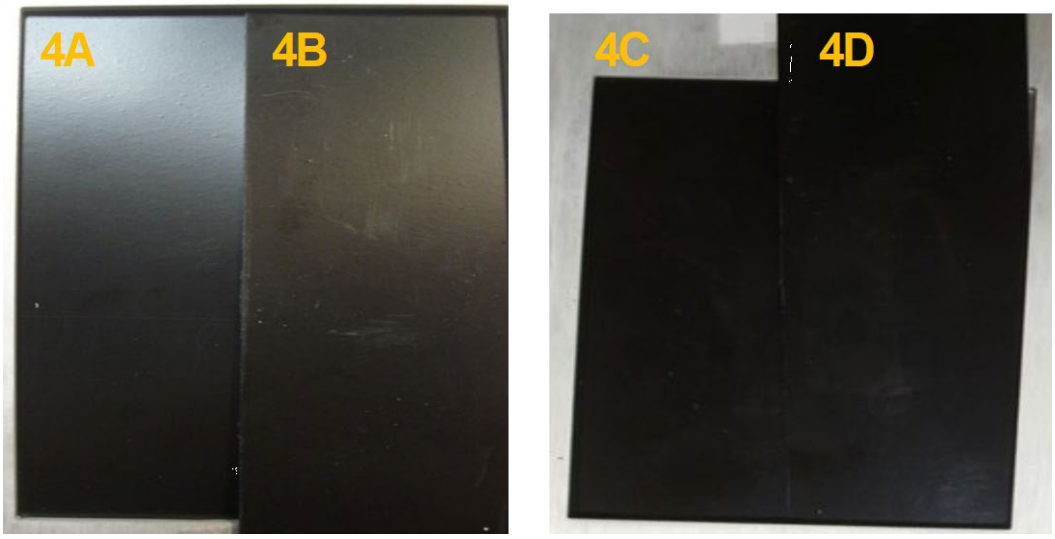

Figure 4. Images of two samples: inside film (A)before and (B) after the UV test; outside film (C) before and (D) after the UV test.

3.2. Real size PV module analysis

3.2.1 Characterization of the PV modules with different encapsulant configurations.

The influence of each new incorporated material over the main PV module electrical parameters is studied in this section. With this aim, real size PV modules with the following four material combinations have been fabricated: STD@White (ten modules), AR@White (ten modules), STD@Black (ten modules) and AR@Black (ten modules). They have been named with correlative numbers followed by its material

combination (see Table 2). The first group corresponds to the most common material combination used for commercial silicon technology, the second group replaces the front STDGlass for ARGlass, the third group varies the white rear protective film for a black one, and the last group changes both the front glass cover and the backsheet. All the real size PV modules have been fabricated in an automatic-assembly-industrial line using PV silicon solar cell with a power range equal to [4.425-4.450) W, without any change in the standard process conditions. The aim of this section is to determine the PV module power difference per evaluated material, with respect to the commercial solar device (STD@White). The unique way to obtain this information is by the lecture of the I-V curve parameters. Therefore, the characteristic of each fabricated PV module has been measured in an industrial PV module solar tester. With the aim of discarding measurement mistakes, each PV module have been measured three times without repositioning in the industrial solar module tester. In order to assure the STD conditions [30], the industrial equipment radiation has been checked with the factory internal working reference module (not shown here). The I-V curve main parameter average values are showed in Table 2 per each PV module together with the average value per each material configuration. These are: short circuit current (I_{sc}) and maximum power point current (I_{mp}), open circuit voltage (V_{oc}) and maximum power point voltage (V_{mp}), the maximum power (P_{mp}), and the fill factor (FF), In addition, the cell to module ratio (CMR) is also indicated. CMR is the relative difference between the measured P_{mp} $(P_{mp})_{measured}$ and the P_{mp} of a PV module fabricated with the same PV cell power range without any performance loss $(P_{mp})_{ideal}$ (Eq. (1). $(P_{mp})_{ideal}$ is determined by the number of cells multiplied by the lowest PV cell power (60 × 4.425) W. Therefore, CMR gives information about the proximity of the PV module performance to ideality.

$$CMR = \frac{P_{mp})_{measured} - P_{mp})_{ideal}}{P_{mp})_{ideal}} \times 100 \qquad Eq.1$$

The first studied PV module group will be considered as the reference for comparison with the new PV modules with the different material combinations. They have been named with correlative numbers, namely Ref 1 to Ref 10. Regarding current parameters, I_{sc} and I_{mp}, they present values with slight variations: the maximum differences from average value are 33 mA and 66 mA respectively, which correspond to relative differences of 0.37% and 0.80%. Voltage parameters also show a low variability in their values, showing deviations of 93 mV and 291 mV from average values (relative differences of 0.25% and 0.95%) for V_{oc} and V_{mp} respectively. Variations in these two voltages can be related with soldering issues, but as no changes have been carried out in this stage, they are more probably due to the PV cell variability in each sorted class. Using this configuration, P_{mp} minimum, maximum and average values are 255.19 W, 256.34 W and 255.70 W which implies a maximum and relative difference equal to 1.15 W and 0.45% respectively. These parameter variations are normal in PV module production line because they are composed by PV cells within the same power range, and this implies slight variations of their I-V curve parameters. These variations at PV cell level are reflected at PV module level and explain the need of sorting PV module production in discrete power intervals of 5.0 W. In this PV module group, all of them are inside the power range [255.00-259.99) W which indicates a proper solar cell classification, together with an adequate PV module process.

The first substituted PV module component has been the front cover glass. Ten PV modules have been fabricated with AR@White combination material, numbered 1_AR@White to 10_AR@White. The introduction of the AR coating reduces the radiation reflection at the front PV cover, which has a direct effect on the current parameters, and through these ones, on the solar device power. Table 2 shows I-V values

per AR@White samples. Regarding I_{sc} parameter, it is possible to observe its general and notable increment. Its minimum, maximum and average values are 9.06 A, 9.12 A and 8.98 A respectively. When comparing I_{sc} average value for this material combination with the standard one (STD@White), a current increment of 200 mA (relative difference equal to 2.21%) has been determined. Obviously, the I_{mp} parameter follows the same trend, and a great increase has been measured. It reaches minimum, maximum and average values of 8.44 A, 8.51 A and 8.05 A respectively. Differences between AR@White and STD@White for I_{mp} average values indicates a current improvement equal to 144 mA (relative difference of 1.71%). Regarding voltage parameter values, V_{oc} and V_{mp} just present slight variations and their average values are 37.98 V and 30.89 V respectively. Their average differences with the reference material combination are 36.42 mV (0.10% relative difference) and 85.08 mV (0.28% relative difference) for V_{oc} and V_{mp} parameters. The former current improvements have a direct effect over P_{mp} parameter, whose minimum, maximum and average values are 260.80 W, 263.50 W and 257.53 W respectively. This implies that the AR coating glass leads to an average increment of 5.11 W (relative difference of 1.96%) and in the most favorable case it supposes an increment of 8.06 W. Regarding the sample with the lower power value, 9_AR@White, it is customary to notice that they are just the current parameters which are slightly different from the rest of the group, while voltage parameter values are very similar for all the PV modules sharing this material combination. This would lead to relate the P_{mp} parameter diminution to a spectral mismatch issue at cell level, better than to a problem during PV module process. Coming back to the general P_{mp} analysis, the former power increments imply that most of the fabricated AR@White PV modules, or even the whole production (in the case of a power enhancement of 5.11 W), will be consider in the immediately above power range than those fabricated according to the STD@White configuration. Finally, these parameter improvements are reflected in CMR parameter whose average value has been reduced from -3.69% to -1.77%.

The third fabricated sample group replaces the white backsheet for a black protective film. The ten PV modules have been named 1_STD@Black to 10_STD@Black. The more affected parameters by this backsheet change are again currents, which has a negative repercussion over the output power. In this case, the income radiation is the same as for the reference PV modules, but all the reflection related with the PV module non-silicon area is lost due to the black backsheet. The minimum, maximum and average values for I_{sc} parameter are 8.66 A, 8.69 A and 8.63 A respectively. When the average value of this material combination is compared with the commercial device average value, a decrease equal to -192 mA (relative difference of -2.21%) can be determined. This current lost is slightly higher for I_{mp} parameter, -227 mA (relative difference of -2.81%). As it was expected, this material change does not influence over voltage parameters, which present average differences of -56 mV and -28 mV (relative differences of -0.45% and -0.09%) for V_{oc} and V_{mp} respectively. The power parameter is really affected and their minimum, maximum and average values are 247.04 W, 248.33 W and 244.54 W respectively which implies an average difference of -8.66 W (relative difference of -3.51%) with respect the standard material configuration. This implies that most of the STD@Black PV modules will be sorted as 245 PV model with its negative economic implications. Regarding the sample with the lower P_{mp} value, 2_STD@Black, its low performance is directly related with V_{mp} and consequently with some problem at soldering stage. It could be a cell breakage or maybe an unsuitable contact between cupper ribbon tab and busbar. Finally, average value of CMR ratio goes down to -6.95%.

The last PV module sample group changes both outer protective films. Ten PV modules with AR@Black material configuration have been fabricated with the same PV nomenclature than before. As it is expected, the more affected parameters are current and power, but the radiation losses related with the black backsheet are absolutely softened by the radiation reflection reduction related with the ARGlass. I_{sc} values present minimum, maximum and average values equal to 8.88 A, 8.90 A and 8.84 A respectively. Its average difference is really insignificant and equal to 21 mA (relative difference of 0.24%). Regarding I_{mp} values, their minimum, maximum and average values measurements are 8.31 A, 8.37 A and 8.29 A respectively. When the former average value is compared with the STD@White average values, a difference of 14 mA has been measured. This suitable optical balance leads to keep the average P_{mp} value at the same level than STD@White power range. Its average value is equal to 255.69 W with a very narrow power range between 255.14 W to 256.39 W. This implies that all the fabricated PV devices with this material configuration will be sorted as 255 W with relevant economic implications. Finally, voltage parameters present stable values and CMR ratio is equal to -3.79%, that is very similar to the standard configuration value.

Encapsulant configuration	Module	I_{sc}(A)	V_{oc}(V)	I_{mp}(A)	V_{mp}(V)	P_{mp}(W)	FF (%)	CMR (%)
STD@White	Ref 1	8.85	37.91	8.29	30.81	255.55	76.18	-3.75
	Ref 2	8.87	37.92	8.30	30.84	255.95	76.11	-3.60
	Ref 3	8.85	37.94	8.30	30.83	255.99	76.24	-3.58
	Ref 4	8.87	37.93	8.34	30.60	255.19	75.85	-3.88
	Ref 5	8.84	37.99	8.30	30.78	255.57	76.11	-3.74
	Ref 6	8.84	37.94	8.30	30.81	255.66	76.26	-3.70
	Ref 7	8.86	37.99	8.30	30.90	256.34	76.17	-3.45
	Ref 8	8.86	37.97	8.27	30.85	255.20	75.85	-3.88
	Ref 9	8.86	37.92	8.29	30.85	255.68	76.11	-3.70
	Ref 10	8.87	37.90	8.30	30.81	255.85	76.10	-3.74
	Average	**8.86**	**37.94**	**8.30**	**30.81**	**255.70**	**76.10**	**-3.69**
AR@White	1_AR@White	9.07	38.00	8.47	30.88	261.50	75.87	-1.51
	2_AR@White	9.07	37.98	8.48	30.70	260.34	75.58	-1.94
	3_AR@White	9.08	38.02	8.47	30.90	261.81	75.86	-1.39
	4_AR@White	9.02	37.99	8.48	30.78	261.04	76.22	-1.68
	5_AR@White	9.12	38.03	8.51	30.92	263.25	75.86	-0.85
	6_AR@White	9.07	37.99	8.50	30.62	260.30	75.57	-1.96
	7_AR@White	9.07	37.99	8.51	30.71	261.28	75.81	-1.59
	8_AR@White	9.04	37.96	8.49	30.65	260.25	75.85	-1.98
	9_AR@White	8.98	37.93	8.05	32.01	257.53	75.66	-3.00
	10_AR@White	9.04	37.91	8.47	30.79	260.75	76.03	-1.79
	Average	**9.06**	**37.98**	**8.44**	**30.89**	**260.80**	**75.83**	**-1.77**
	Average Difference					5.11		
	Maximum Difference					8.05		
STD@Black	1_STD@Black	8.64	37.97	8.08	30.98	248.33	75.67	-6.47
	2_STD@Black	8.67	37.86	8.06	30.57	244.54	74.50	-7.89
	3_STD@Black	8.67	37.91	8.07	30.92	247.58	75.31	-6.75
	4_STD@Black	8.63	37.89	8.06	30.91	247.11	75.57	-6.93
	5_STD@Black	8.68	37.87	8.06	30.84	246.79	75.11	-7.05
	6_STD@Black	8.69	37.83	8.07	30.84	247.09	75.16	-6.93
	7_STD@Black	8.68	37.86	8.07	30.89	246.95	75.13	-6.99
	8_STD@Black	8.65	37.85	8.07	30.88	247.33	75.57	-6.84
	9_STD@Black	8.65	37.90	8.14	30.67	247.74	75.55	-6.69
	10_STD@Black	8.68	37.92	8.06	30.88	246.91	75.00	-7.00
	Average	**8.66**	**37.88**	**8.07**	**30.84**	**247.04**	**75.26**	**-6.95**
	Average Difference					-8.66		
	Maximum Difference					-11.80		
AR@Black	1_AR@Black	8.90	37.91	8.30	30,77	255.45	75.70	-3.78
	2_AR@Black	8.89	37.93	8.37	30.56	255.72	75.87	-3.68
	3_AR@Black	8.86	37.95	8.32	30.68	255.34	75.97	-3.83
	4_AR@Black	8.87	37.93	8.31	30.79	255.80	76.05	-3.66
	5_AR@Black	8.88	38.00	8.31	30.85	256.39	76.01	-3.43
	6_AR@Black	8.91	37.95	8.31	30.75	255.59	75.57	-3.73
	7_AR@Black	8.88	37.94	8.31	30.83	256.21	76.02	-3.50
	8_AR@Black	8.84	37.95	8.29	30.83	255.73	76.20	-3.68
	9_AR@Black	8.87	37.94	8.30	30.79	255.51	75.89	-3.76
	10_AR@Black	8.87	37.96	8.31	30.71	255.14	75.75	-3.90
	Average	**8.88**	**37.95**	**8.31**	**30.76**	**255.69**	**75.90**	**-3.70**
	Average Difference					-0.01		
	Maximum Difference					-1.20		

Table 2. I–V curve for photovoltaic modules with the four possible material combinations: STD@White, AR@White, STD@Black and AR@Black

3.2.2. Accelerated PV module aging test.

The objective of this section is to study the PV module behavior under the main accelerated aging test: humidity freeze (HF), thermal cycles (TC) and damp heat (DH) [24]. Due to the climate chamber availability (both spatial and temporal) and to the purpose of this work, which is to determine the convenience (or not) of the front and rear cover material changes, not all the fabricated PV modules have been aged, as it is shown in Figure 1. Just modules belonging to the series with AR@White and AR@Black material combinations have been degraded. The AR@White sample (1_AR@White module) will provide information about the ARGlass evolution, because the white backsheet behavior is well known at industrial level. The AR@Black material combination sample (5_AR@Black module) will give us information about two mean issues: firstly, the evolution of the new black backsheet, and secondly the interaction between the two new materials. The obtained results are shown in Table 3. The incorporation of these two materials has strong economic implications for a factory, therefore, such technical decision has to be firmly supported. It is worth mentioning here that prior to the aging test, both PV modules have been exposed to the natural light during a month with the aim to perform the typical silicon solar cell sudden degradation. This explains the non-degraded PV module I-V curve parameter differences between Table 2 and Table 3.

The aging test that may lead to a higher material degradation is DH test. In this case, it is going to be registered with a high accuracy level for the two PV modules 1_AR@White and 5_AR@Black, plus an additional one, the 4_AR@Black. The cycling has been stopped two times along the total degradation time of 1000 hours. The obtained results are shown in Table 4.

I-V curve measurements are the selected technique to report the aging test results, on the basis of its comparison before and after the test. In such type of I-V curve analysis, the calibration and verification of the solar module tester becomes a relevant factor, since several weeks pass between the beginning and the end of the aging test. In our case, the solar PV module tester is that used in the commercial production line; therefore, their production calibration and verification protocols guarantee the measurement accuracy during and at the end of the aging cycles [22]. Besides, in order to have a visual detail of the PV module appearance, electroluminescence (EL) images have been recorded before and after the test.

The experimental data have been distributed in two tables, Table 3 and Table 4, where I-V curve parameters of the production reference module (named as PR) and the working reference module (WR) are also showed. Obviously these two PV modules are not submitted to the aging tests. PR module is used as reference for commercial product production. This PV reference is generated from a “zero-level reference”, this is a PV module calibrated from a certified company (which is never used in the production line and it is not shown here). PR module is subjected to reference module renovation protocol in the factory. With the aim to avoid any uncertainty in the module tester calibration, a second reference module has been assigned to this evaluation, and this is named WR. Both PV module references are always measured prior to the measurements of the aged modules under study in this work, and the production verification criterion is applied. This verification criterion is based on P_{mp} values and it accepts an uncertainty of ± 0.50% for the WR certified value. In the case of higher power variation, the solar simulator irradiation must be re-calibrated. The WR P_{mp} certified value is equal to 247.60 W. Therefore, the accepted power uncertainty range is [246.36-248.84] W. As WR power values showed in Table 3 and Table 4 never exceed this verification power range, a specific irradiation calibration has not been necessary during the running of this aging

process. This means that the solar module tester always works under the STC measurement conditions (1000 W/m^2 of illumination and 25 °C of temperature), agreeing thus the international normative (IEC 60904) [30].

Coming back to the aging test analysis, they are based on a relative power loss pass/fail criterion equal to 5% [28]. With the aim to obtain accurate I-V curve parameters, each studied PV module is measured three times and their average parameter values are showed in Table 3 and Table 4. The P_{mp} value of each PV module under study is corrected using the WR certified value. This correction is calculated using the equation [2] where P_{mp_Corr} and P_{mp} are the corrected P_{mp} value, and the power measured of the module under study, respectively; P_{mp_WR} is the power measured of the module WR and 247.60 is the WR P_{mp} certified value. Finally, relative differences and accumulative relative differences are determined per each performed aged test.

$$P_{mp\_Corr} = P_{mp} - P_{mp} \cdot \left(\frac{P_{mp\_WR} - 247.60}{247.60}\right) \qquad Eq.(2)$$

3.2.2.1. Humidity Freeze test

In this case, the first performed accelerated aging test has been HF because it was the running test in the climate chamber when this experiment began. Regarding 1_AR@White sample, it can be observed that all the I-V curve parameters maintain very similar values to those measured before test. In the case of P_{mp} parameter its variation is practically negligible, from 256.68 W to 256.80 W, exactly a relative difference of 0.04% with respect to the undegraded situation. The 5_AR@Black module behavior is very similar. Indeed, its power decreases from 253.42 W to 253.21 W, which implies a relative difference of -0.08%.

3.2.2.2. Damp Heat test

The second performed test is DH test, which is the most suitable test to evaluate the material reliability against environmental degradation due to its extreme temperature and humidity conditions, which can promote the moisture ingress process across the backsheet. The relevance of this test for evaluate our material behavior has lead us to perform a more detailed analysis along test length. On one hand, an additional AR@Black material combination module (4_AR@Black sample) has been also degraded. On the other hand, the climate chamber cycle has been stopped two times along the 1000 hours of DH cycle duration. Table 3 shows the final results and Table 4 presents this detailed view for the three modules. The first stop is made after 430 hours of DH test and Table 4 shows the I-V curve results for the three modules. Electrical parameters allow to observe that both 1_AR@White and 4_AR@Black modules present a slight variation, where relative differences in P_{mp_Corr} can be quantified as 0.46% and 0.47% respectively. On the contrary, 5_AR@Black sample exhibits a higher power variation because its corrected power decreases from 257.86 W to 253.10 W (a relative difference of -1.30%). Next stop happened at 883 hours of DH test. Again 1_AR@White and 4_AR@Black samples show a quasi-negligible degradation because their corrected power pass from 253.10 W and 249.36 W, to 256.35 W and 253.24 W respectively. These values suppose accumulative relative differences equal to -0.13% and 0.52% respectively. In the case of the 5_AR@Black sample, the degradation is more evident because the corrected power goes down to 248.25 W, and the accumulative relative difference is -1.74%. At the end of the DH cycle the three modules follow the observed trend and the final accumulative differences are -0.92%, -0.38% and -2.33% for 1_AR@White, 4_AR@Black and 5_AR@Black samples respectively.

3.2.2.3. Thermal Cycling test

The final aging test is TC, where the same two modules implicated on the whole degradation process have been analyzed. The 1_AR@White I-V parameters show a notable reduction when compared to those obtained after the previous DH test. With the aim to have a general view of the degradation process suffer by this configuration, the results after TC test should be better compared with non-degraded values. This analysis reveals that for 1_AR@White sample, current values suffer a reduction around -200 mA and the higher voltage losses, -370 mV, happens to V_{mp} values. These parameter decrements lead to reduce the P_{mp} value to 248.20 W which supposes an accumulative difference equal to -3.31 %. In the case of 5_AR@Black sample, it suffers a current degradation of -130 mA and -270 mA for I_{sc} and I_{mp} parameters, but the higher decrease has been detected for V_{mp} value, and it is equal to -1000 mV. This led to a total corrected P_{mp} variation from 253.42 W to 240.97 W, which implies an accumulative relative difference of -4.91%.

Therefore, both material configurations overcome the regulated aging process, since the final values of accumulative relative differences do not surpass the fixed power loss criterion (5%) [28]. Nevertheless, AR@White combination degradation values are very similar to those obtained for other encapsulant materials (-2.97% for new ethilen-vynil-acetate materials [22]), although AR@Black material combination figures exceed this value.

Material configuration	Aging Test	Module	Isc(A)	Voc(V)	Imp(A)	Vmp(V)	FF (%)	Pmp(W)	Pmp_Corr(W)	Relative difference (%)	Accumulative relative difference (%)
AR@White	Before Test	PR	8.52	37.211	7.99	29.57	74.51.	236.29			
		WR	8.66	37.64	8.13	30.47	75.97	247.74			
		1_AR@White	9.01	38.08	8.39	30.61	74.89	256.83	256.68		
	10 HF	PR	8.50	37.11	7.97	29.89	75.55	238.28			
		WR	8.66	37.65	8.11	30.44	75.76	247.01			
		1_AR@White	8.99	38.04	8.38	30.58	74.81	256.19	256.80	0.04	
	1000 h DH	PR	8.49	37.12	7.97	29.85	75.41	237.80			
		WR	8.66	37.65	8.11	30.44	75.77	246.90			
		1_AR@White	8.82	37.95	8.28	30.66	75.81	253.70	254.43	-0.92	
	200 TC	PR	8.47	37.10	7.95	29.88	75.59	237.58			
		WR	8.62	37.56	8.10	30.50	76.26	247.04			
		1_AR@White	8.83	38.03	8.10	30.24	73.73	247.63	248.20	-2.45	-3.31
AR@Black	Before Test	PR	8.50	37.13	7.97	29.90	75.53	238.38			
		WR	8.62	37.56	8.10	30.50	76.24	246.98			
		5_AR@Black	8.85	38.06	8.24	30.67	75.07	252.79	253.42		
	10 HF	PR	8.52	37.21	7.99	29.57	74.51	236.29			
		WR	8.62	37.56	8.10	30.50	74.91	246.98			
		5_AR@Black	8.83	38.22	8.19	30.82	74.85	252.58	253.21	-0.08	
	1000 h DH	PR	8.49	37.12	7.97	29.85	75.41	237.80			
		WR	8.65	37.65	8.11	30.44	75.77	246.89			
		5_AR@Black	8.71	38.04	8.08	30.50	74.46	246.57	247.28	-2.34	
	200 TC	PR	8.47	37.10	7.95	29.88	75.59	237.58			
		WR	8.62	37.56	8.10	30.50	76.31	246.44			
		5_AR@Black	8.72	38.08	7.97	29.67	71.21	239.86	240.99	-2.54	-4.91

Table 3. I-V curve results for the most typical aging test: damp heat, thermal cycle and humidity freeze aging test according to IEC 61215 normative. PR: production reference; WR: working reference.

Time (h) Damp Heat Test	Module	I_{sc}(A)	V_{oc}(V)	I_{mp}(A)	V_{mp}(V)	FF (%)	P_{mp}(W)	P_{mp_corr}(W)	Rel. Dif (%)	Accumulative relative difference (%)
	PR	8.50	37.11	7.97	29.89	75.55	238.28			
	WR	8.66	37.65	8.11	30.44	75.76	247.01			
0	1_AR@White	9.01	38.08	8.39	30.61	74.89	256.83	256.68		
	4_AR@Black	8.84	38.04	8.24	30.60	74.93	252.06	251.92		
	5_AR@Black	8.85	38.06	8.24	30.67	75.07	252.79	253.21		
	PR	8.50	37.13	7.97	29.90	75.53	238.38			
	WR	8.66	37.66	8.14	30.51	76.16	248.29			
430	1_AR@White	8.98	37.99	8.38	30.86	75.76	258.58	257.86	0.46	0.46
	4_AR@Black	8.83	37.91	8.22	30.85	75.83	253.81	253.10	0.47	0.47
	5_AR@Black	8.80	38.08	8.17	30.61	74.66	250.06	249.36	-1.30	-1.30
	PR	8.50	37.08	7.97	29.86	75.50	237.97			
	WR	8.66	37.63	8.14	30.39	75.82	247.19			
883	1_AR@White	8.83	37.96	8.31	30.79	76.34	255.93	256.35	-0.58	-0.13
	4_AR@Black	8.81	37.92	8.21	30.78	75.68	252.82	253.24	0.05	0.52
	5_AR@Black	8.73	38.05	8.12	30.52	74.59	247.84	248.25	-0.44	-1.74
	PR	8.49	37.12	7.97	29.85	75.41	237.80			
	WR	8.65	37.65	8.11	30.44	75.77	246.89			
1000	1_AR@White	8.82	37.95	8.28	30.66	75.81	253.70	254.43	-0.75	-0.92
	4_AR@Black	8.79	37.93	8.19	30.80	75.59	252.14	252.86	-0.14	-0.38
	5_AR@Black	8.71	38.04	8.08	30.50	74.46	246.57	247.28	-0.39	-2.33

Table 4. I-V curve results for the progressive damp heat aging test according to IEC 61215. PR: production reference; WR: working reference.

3.2.2.4. Electroluminiscence results

With the aim to have more information about PV module degradation, EL images (Figure 5) have been taken for two modules before and after the aging test: 1_AR@White (Figure 5A and 5A*, before and after the cycles respectively) and 5_AR@Black (Figure 5B and 5B*, before and after the process respectively). Four different defects with different origins have been detected in both aged PV samples which have been marked as follows: broken fingers (green triangles), diagonal black lines (red circles) and two large inactive areas (yellow and blue rectangles). Broken fingers are related to PV cell front metallization issues: unsuitable silver past dosage or palette uneven. Diagonal black lines are a clear signal of a PV cell breakage, -although without a relative displacement of the two separated pieces-, avoiding the contact between the n-type and p-type parts. When this displacement happens, a dark region can be observed, and an inactive area is defined. These inactive areas use to have a clear origin related with an excessive welding pressure, these defects start at one of the frontal busbars (welding point), and they can extent to the PV cell edge, describing a triangle shape. Large inactive areas are marked with yellow and blue rectangles. In this study, the yellow one indicates an unsuitable contact between the busbar and the copper tab ribbon, and the blue one indicates a probable PV cell degradation or even some problem related with the encapsulant material. As can be observed, non-degraded PV modules just show broken fingers randomly distributed over the PV module surface. Moreover, in the case of 1_AR@White sample, a PV cell breakage can be observed.

From a general point of view, it can be observed that due to the aging process there is a significant increase in the number of broken fingers in both modules. This is the most common defect and just few of them have been indicated by the green triangles in Fig. 5. Regarding diagonal black lines, they are also presented in both studied solar devices (red circles). They are always related with cell breakage but just in some cases the final effect is its progression to a dark region, because the lamination mechanical stability often prevents this effect. The commented dark region only takes place when there is a vertical displacement of the broken sections and one part is disconnected from the rest of the solar device. The most impressive defects are the black regions marked with colored rectangles. The yellow rectangle has only been detected at 5_AR@Black

module. It indicates an unsuitable contact between the busbar and the copper tab ribbon, despite of the pressure ejected by the lamination and the glass cover. This explains the I-V curve measured variations, mainly the 1.00 V drop detected in V_{mp} parameter. Regarding the blue rectangles (observed in both modules), they are related with the encapsulant degradation due to moisture ingress process. Nevertheless, its power implications are limited because it is also presented in the sample with the lower power loss (1_AR@White module).

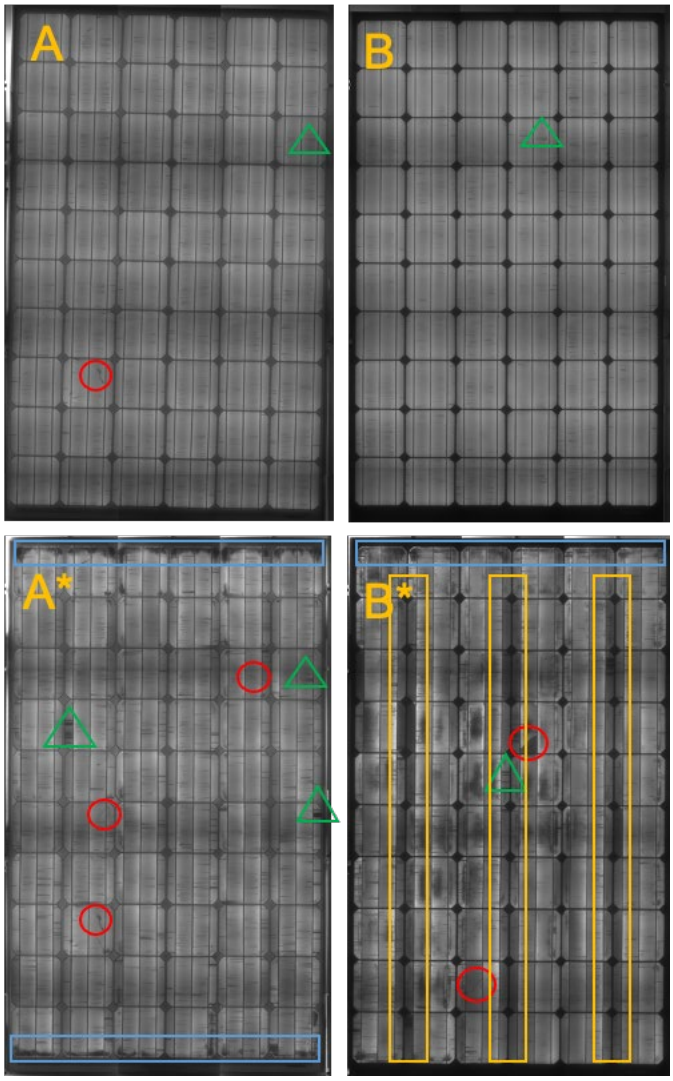

Fig. 5. Electroluminescence images of the PV modules mounted with the following material combinations: (A) AR@White before the aging test and (A*) after the whole aging process; (B) AR@Black material before the aging test and (B*) after the whole aging process. Inactive areas: blue and yellow rectangles; cell breakage: red circles; metallic serigraphy defects: green triangles. (For interpretation of the references to color in this figure legend, the reader is referred to the web version of this article).

3.2.3. Production capacity and economic impact of the PV module material combination

This section is devoted to the energy yield and economic study of the four material combinations when they are implemented in a real factory. More specifically, PV modules production results from a fully automatic module assembling line with a production capacity equal to 110 MW per year (400 devices per shift; a daily production of 1200 solar modules; 438,000 PV modules per year) have been used for this task. A real STD@White PV module production database is managed and the previously determined power variations are implemented in this real PV module power range distribution. In this case, data from a week of production, 7568 units, whose power range distribution is showed in Figure 6, is considered in this analysis. The STD@White power range histogram shows a narrow PV module distribution, where the majority of the produced devices are concentrated in three PV module models: 245 W (1.36%), 250 W (82.49%) and 255 W (16.07%). Such distribution indicates a suitable PV cell classification and a well-controlled PV module process.

When the STDGlass is substituted by the ARGlass, an average power increment equal to 5.11 W has been measured (see Table 2), and the corresponding PV module range distribution result is showed in Figure 6 (second histogram). In this case, almost the whole distribution moves toward the following PV module model, because the power increment is slightly higher than the power interval of 5.00 W. This implies that AR@White material combination will be able to center its production on 255W PV model (79.44%), and even obtain 260W PV model in an appreciable quantity (19.16%).

The STD@Black combination leads to an average reduction of -8.66 W because the non-silicon material reflectance is almost totally annulled (see Table 2). In this case, the possible histogram is moved towards lower PV module models and it is quite broader than the former two, because the power reduction is higher than the used power interval of 5.00 W. The three main obtained products are 240 W, 245 W and 250 W with percentages equal to 32.12%, 67.24% and 0.03% respectively.

Finally, AR@Black design power variation has been implemented on the real production database. As the power variation is -0.01 (see Table 2), an inappreciable production histogram variation is obtained. The 250 W PV module model is recovered as the main one, and 255 W PV module model is processed in a percentage equal to 15.75%.

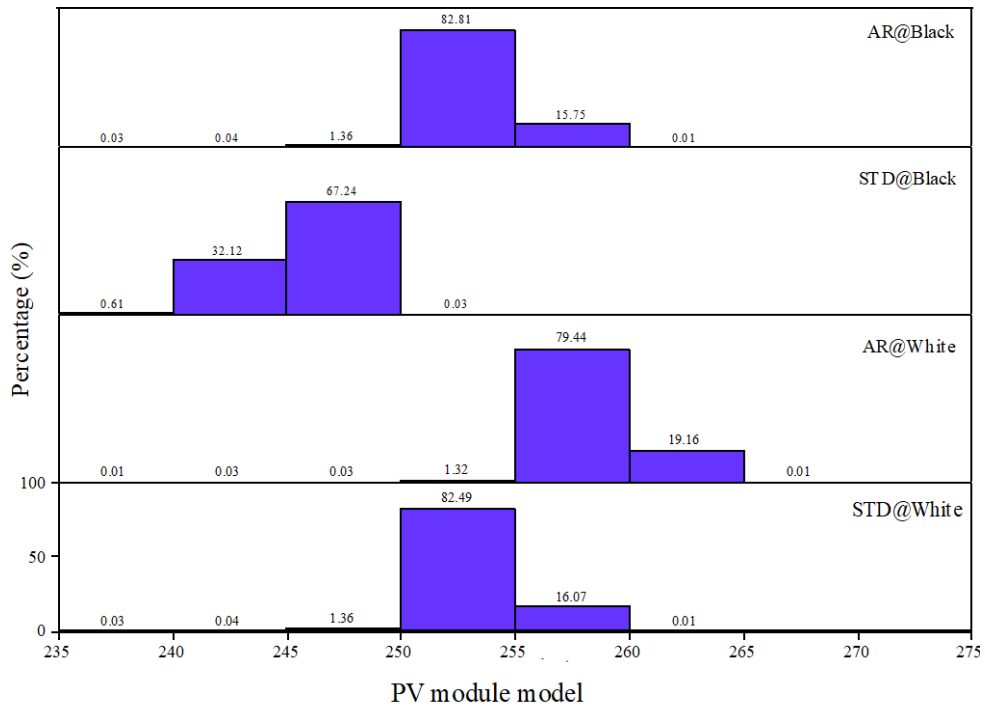

Fig 6. Real PV module model distribution for four possible PV module combination. (First) STD@White; (Second) AR@White; (Third) STD@Black and (Fourth) AR@Black

The material design implementation over the real production line will also have a sale income impact, which is going to be analyzed in this subsection. Table 5 shows the production capacity and the economic variations per material combination using as reference 100 MW per year with STD@White material configuration. The considered retailed price is equal to US \$0.57 W_p [33] for STD@White, AR@White and STD@Black configurations, while in the case of AR@Black material design, a prize increment of 20% [34] is considered, due to its aesthetic improvement (US \$0.650 W_p). Both prices are tax excluded and the repercussion of a possible differences in material cost is also omitted. Table 5 indicates that 90.33 MW of the whole production capacity belongs to 250W PV module model when STD@White is the processed material combination, which implies a sale income equal to US \$48.96 M for this PV module model. Taking into account all the module models, the sale income reaches US \$59.52 M per year. Nevertheless, if an AR-Glass front cover is used, it is possible to obtain a similar year production capacity, but 88.73 MW lie in the upper PV module model, which supposes a year sale income of US \$48.09 M per year. Moreover, the extension of the PV module power range until 260W for a considerable number of PV module units, leads the AR@White configuration sale income up to US \$60.75 M per year. When comparing this data with the corresponding to the STD@White configuration, the sale income increase is US \$1.23 M per year without any machinery change and only by using a suitable handling system protection.

STD@Black is the third material combination examined. In this case, a notable reduction can be observed in both, power module and sale incomes. The PV module model dramatically drops to 240W and 245W with year production capacities per model equal to 33.76 MW and 72.15 MW respectively. Regarding its whole sale income, it is equal to US \$57.77 M which implies a loss of US \$1.75 M.

The last AR@Black module configuration allows to balance the production capacity and also the economic impact. With respect to the production capacity, the 250 W PV module model has been recovered as the main produced product followed by 255 W. Obviously, this power situation together with the final price increment in 20% [34] allows to promote the sale incomes until US \$71.42 M, this is an estimative extra of US \$11.90 M per year.

PV MODULE MODEL	PRODUCTION CAPACITY (MW per year) MATERIAL DESIGN				PV MODULE RETAILER PRICE: US \$0.542 Wp (US \$ million per year) MATERIAL DESIGN			
	STD@White	AR@White	STD@Black	AR@Black	STD@White	AR@White	STD@Black	AR@Black*
235	0.03	0.01	0.63	0.03	0.02	0.01	0.34	0.02
240	0.04	0.03	33.76	0.04	0.02	0.02	18.30	0.03
245	1.46	0.03	72.15	1.46	0.79	0.02	39.11	0.95
250	90.33	1.44	0.03	90.68	48.96	0.78	0.02	58.98
255	17.95	88.73		17.59	9.73	48.09		11.44
260	0.01	21.82		0.01	0.01	11.83		0.01
265		0.01				0.01		
Σ					59.52	60.75	57.77	71.42

Table 5. Production capacity and economic impact for STD@White and AR@Black PV module material combination.

4. Conclusions

A successful highly architecture integrated PV module has been fabricated with inappreciable power losses by a suitable material combination. The innovate design implies antireflective coating glass (ARGlass) instead of the standard one (STDGlass), and black backsheet instead of the white one, in order to give rise to the most aesthetic PV module (AR@Black configuration).

Previous to the in line new materials implementation, they have been independently analyzed. Transmittance measurements have been carried out over STDGlass and ARGlass, and they determine a transmittance increment from 87.42% to 95.73% at 700 nm respectively. The suitability of the adhesion between EVA and black backsheet has been determined in three samples by the peel test and their strength measurements are equal to 63.34 N/cm^2, 115.04 N/cm^2 and 143.33 N/cm^2 which are higher than the recommended supplier value of 30.00 N/cm^2. The EVA cure grade is determined by gel content test in three samples whose values vary from 39% to 59%. The last individual sample test carried out has been backsheet ultraviolet degradation and no aesthetic defect has been detected.

Real size photovoltaic modules with STD@White (reference), AR@White, STD@Black and AR@Black material combinations have been successfully fabricated in the automatic industrial line with cotton gloves handle protection. Regarding their power differences with respect to the AR@White reference, STD@Black and AR@Black designs present variations equal to +5.11 W, -8.66 W and +0.01 W respectively. This implies that AR@Black combination leads to fabricated PV modules which join high solar energy conversion with a high building integration material design Regarding accelerating aging tests, they have been accomplished for modules having the material combinations with the higher building integration possibilities: AR@White and AR@Black. I-V curves measurements prior and after the test have allowed to determine AR@White and AR@Black power relative variations which are 0.04% and -0.08% for humidity freeze test, -0.92% and -2.34% for damp heat test and -2.45% and -2.54% for thermal cycle test respectively. This implies that, the total relative degradation can be quantified as 3.31% for AR@White and 4.91% for AR@Black modules. These values indicate that both individual and overall values of power relative variation are lower than the assumed pass/fail criterion of ± 5%. Therefore, our studies allow to conclude that the AR@Black material combination can be used for high building integration PV modules without any power loss.

Finally, the economic impact of these most relevant combinations have been evaluated for a production capacity of 110 MW per year and a real production distribution, which originally is laminated with STD@White design. The typical material combination implies a gross income of US $59.52 M (module retailed price of US $0.542 W_p) while the new AR@White combination would lead this value to US $60.75 M and AR@Black US $74.40 M (25% module related price increment) which suppose an estimative extra of US $1.23 M for AR@White and US $14.88 M for AR@Black per year.

Acknowledgements

The authors are thankful to ISOFOTON S.A. and J. Alcaide and J. Rando from 4TENERGY S.COOP:AND, for their collaboration.

References

[1] A.B. Kristiansen, T. Ma, R.Z. Wang, Perspectives on industrialized transportable solar powered zero energy buildings, Renew. Sust. Energ. Rev.2019;108:112-124.
[2] M. Li, T. Ma, J. Liu, H. Li, Y. Xu, W. Gu, L. Shen. Numerical and experimental investigation of precast concrete façade integrated with solar photovoltaic panels. Appl. Energy 2019;253:113509.
[3] P. Jayathissa, M. Jansesn, N. Heeren, Z. Nagy, A. Schulueter. Life cycle assessment of dynamic building integrated photovoltaics. Sol Energy Mater Sol Cells 2016;156:75-82.
[4] M.A. Butturi, F. Lolli, M.A. Sellitto, E. Balugani, R. Gamberini, B. Rimini, - Renewable energy in eco-industrial parks and urban-industrial symbiosis: A literature review and a conceptual synthesis. Appl Energy 2019;255: 113825.
[5] Y. Luo, L. Zhang, Z. Liu, J. Yu, X. Xu, X. Su, Towards net zero energy building: The application potential and adaptability of photovoltaic-thermoelectric-battery wall system. Appl Energy 2020;258: 114066.
[6] Y.B. Assoa, L. Gaillard, Ch. Ménézo, N. Negri, F. Sauzedde. Dynamic prediction of a building integrated photovoltaic system thermal behavior. Appl Energy 2018;214:73-82.
[7] M. Tripathy, H. Joshi, S.K. Panda. Energy payback time and life-cycle cost analysis of building integrated photovoltaic thermal system influenced by adverse effect of shadow. Appl Energy 2017;200:376-389.
[8] Z. Hu, W. He, J. Ji, D. Hu, S. Lv, H. Chen, Z. Shen, Comparative study on the annual performance of three types of buildings integrated photovoltaic (BIPV) Trombe wall system. Appl Energy 2017;194:81-93.
[9] S. Kurtz, Solar surfaces: A bad idea or tomorrow's mainstream application?. MRS Energy & Sustainability: A Review Journal 2019;6:1-8.
[10] A. Anctil, E. Lee, R. R. Lunt. Net energy and cost benefit of transparent organic solar cells in building-integrated applications. Appl Energy 2020;261:114429.
~~[11] G. Li, Q. Xuan, M.W. Akram, Y. G. Akhlaghi, H. Liu, S. Shittu. Building integrated solar concentrating systems: A review. Appl Energy 2020;260:114288.~~
[12] A. Scognamiglio, H.N. Rostvik, Photovoltaic and zero energy buildings: a new opportunity and challenge for design. Prog. Photovolt: Res. Appl. 2013;21:1319-1336.
[13] V. Kosoric, H.Huang, A. Tabalda, S. Lau, H.T.W. Tan, Survey on the social acceptance fo the productive façade concept integrating photovoltaic and farming systems in high-rise public housing blocks in Singapore. Renew. Sust. Energ. Rev.2019;111:197-214.
[14] M. Pagliaro, R. Ciriminna, G. Palmisano. BIPV: merging the photovoltaic with the construction industry, Prog. Photovolt: Res. Appl. 2010;18:61-72.
[15] M.J.R. Perez, V. Fthenakis, H-Ch. Kim, A.O. Pereira, Façade-integrated photovoltaics: a lif cycle and performance assessment case study. Prog. Photovolt: Res. Appl. 2012. DOI: 10.1002/pip/1167.
[16] Commercial black PV module datasheet [Online]. Available http://www.vicoexport.com/wp-content/uploads/2015/06/isofoton-ISF-Black-240w-245w-250w-vico-export-solar-energy.pdf [accessed: 24-April-2020].
[17] G. Makrides, M. Theristis, J. Bratcher, J. Pratt, G. E. Georghiou. Five-year performance and reliability analysis of monocrystalline photovoltaic modules with different bakchseet materials. Sol Energy 2018;171:491-499.
[18] H.K. Raut, A.S. Nair, S.S. Dinachali, V.A. Ganesh, T.M. Walsh, S. Ramakrishna, Porous SiO2 anti-reflective coatings on large-area substrates by electrospinning and their application to solar modules, Sol. Energy Mater. Sol. Cells 2013;111:9–15.

[19] L.K. Verma, M. Sakhuja, J. Son, A.J. Danner, H. Yang, H.C. Zeng, C.S. Bhatia, Self- cleaning and antireflective packaging glass for solar modules, Renew. Energy 2011;36:2489–2493.
[20] J. Deubener, G. Helsch, A. Moiseev, H. Bornhöft, Glasses for solar energy conversion systems, J. Eur. Ceram. Soc. 2009;29:1203–1210.
[21] S. Jalaly, M. Vahdani, M. Shahabadi, G. Mir Mohamad Sadeghi, Design, fabrication, and measurement of a polymer-based anti-reflection coating for improved performance of a solar panel under a specific incident angle Sol. Energy Mater. Sol. Cells 2019;189:175-180.
[22] M.C. Lopez-Escalante, M. Fernández-Rodríguez, L.J. Caballero, F. Martín, M. Gabás, J.R. Ramos-Barrado. Novel encapsulant architecture on the road to photovoltaic module power output increase. Appl Energy 2018;228:1901-1910.
[23] Commercial black PV module datasheet [Online]. Available https://www.yumpu.com/en/document/view/22115702/ecoguard-float-data-sheet-pdf-guardian-industries [accessed: 24-April-2020]
[24] Glass technical datasheet [Online]. Available <http://023app01.guardian.com/cs/groups/guardianeurope/documents/web_content/stg_031420.pdf [accessed: 16-March-2020]
[25] Backsheet technical datasheet [Online]. Available < https://es.enfsolar.com/pv/backsheet-datasheet/53 [accessed: 24-April-2020]
[26] Ch. Hirschl, M. Biebl-Rydlo, M. DeBiasio, W. Mühleisen, L. Neumaier, W. Scherf, G. Oreski, G. Eder, B. Chernev, W. Schwab, M. Kraft. Determining the degree of crosslinking of ethylene vinyl acetate photovoltaic module encapsulants- A comparative study. Sol Energy Mater Sol Cells 2013;116:203-218.
[27] Ch. Hirschl, L. Neumaier, S. Puchberger, W. Mühleisen, G. Oreski, G.C. Eder, R. Frank, M. Tranitz, M. Schoppa, M. Wendt, N. Bogdanski, A. Plösch, M. Kraft. Determination of the degree of ethylene vinyl acetate crosslinking via Soxhlet extraction: Gold standard or pitfall? Sol Energy Mater Sol Cells 2015;143:494-502.
[28] IEC 61215-2. Terrestrial photovoltaic (PV) modules – Design qualification and type approval – Part 2: test procedures.
[29] EVA technical datasheet [Online]. Available < http://www.evasa.net/w/standard-cure-sc100041ea/ > [accessed: 24-April-2020]
[30] IEC 60904-3 (Ed. 2). Photovoltaic devices – Part 3: Measurement principles for terrestrial photovoltaic (PV) solar devices with reference spectral irradiance data; 2008.
[31] < https://www.ul.com/search#stq=pid&stp=1.pdf > [accessed: 24-April- 2020]
[32] M.C. López-Escalante, L.J. Caballero, F. Martín, M. Gabás, A. Cuevas, J.R. Ramos-Barrado, Polyolefin as PID-resistant encapsulant material in PV modules, Sol. Energy Mater. Sol. Cells 2016;144:691–699.
[33] Retailed price [Online]. Availabe <http://pvinsights.com/RetailerPrice.php> [accessed: 24-April-2020].
[34] Wholesale PV module price [Online]. Available https://suministrosdelsol.com/es/24-paneles-60-celulas [accessed: 24-April-2020].